

Assessment of the universal pattern
decomposition method using MODIS and
ETM+ data

L.Zhang, N.Fujiwara, S.Furumi, K.Muramatsu,
M.Daigo, and L.P.Zhang

2005.4.11

Assessment of the universal pattern decomposition method using MODIS and ETM+ data

L. Zhang¹, N. Fujiwara², S. Furumi³, K. Muramatsu^{3,4}, M. Daigo⁵, and L. Zhang¹

1 LIESMARS, Wuhan University, 129 Luoyu Road, Wuhan 430079, P. R. China

2 Laboratory of Nature Information Science, Department of Information and Computer Sciences, Nara Industrial University, Nara, Japan

3 Laboratory of Nature Information Science, Department of Information and Computer Sciences, Nara Women's University, Nara, Japan

4 KYOUSEI Science Center for Life and Nature, Nara Women's University, Nara, Japan

5 Department of Economics, Doshisha University, Kyoto, Japan

Abstract. The universal pattern decomposition method (UPDM) is a sensor-independent method in which each satellite pixel is expressed as the linear sum of fixed, standard spectral patterns for water, vegetation and soil. The same normalized spectral patterns can be used for any satellite sensor. Supplementary patterns are included when necessary. The UPDM has been successfully applied to simulated data for Landsat/ETM+, Terra/MODIS, ADEOS-II/GLI and 92 bands-CONTINUE sensors using ground-measured data. This paper validates the UPDM using MODIS and ETM+ data acquired over the Three Gorges region of China. The reduced χ^2 values of selected area D, that with the smallest terrain influences, are 0.000409 (MODIS) and 0.000181 (ETM+), and the average linear regression factor between MODIS and ETM+ is 1.0077, with rms 0.0082. The linear regression factor for the VIUPD between MODIS and ETM+ data of area D is 1.0089 with rms 0.0696. Both UPDM coefficients and the vegetation index (VIUPD) are sensor-independent.

1. Introduction

Multi-temporal and multi-sensor satellite data supply a wealth of information for monitoring environmental changes at regional, continental, and global scales. Past studies have focused on terrestrial land cover, vegetation classification (Muchoney *et al.*, 2000), and natural calamities. In addition, satellite data commonly add to studies in oceanography, hydrology, geology, forestry, and meteorology. Larger volumes of multi-spectral data have become available from Landsat/TM (ETM+), Terra (Aqua)/MODIS, ADEOS-II/GLI and other sensors. The characteristics of each sensor differ, as the number of bands, the band wavelengths and the central wavelength of each band vary by satellite (Zhang *et al.*, 2004). Thus, multisensor products must incorporate sensor dependencies. Such dependencies are extremely disadvantageous for global change research (Teillet *et al.*, 1997).

The universal pattern decomposition method (UPDM) is a sensor-independent method that is tailored for satellite data analysis. Sets of spectral reflectance measured by a sensor are transformed by

the UPDM into three or four coefficients with three or four fixed spectral reflectance patterns. Spectral reflectance patterns are determined in the spectral region between 350 nm and 2500 nm and are called the “universal standard spectral patterns.” Sensor wavelength values are selected from the universal standard spectral patterns to analyze the spectral region of each sensor. The coefficients are “pattern decomposition coefficients.” This method has been successfully applied to simulated data with wavelengths observed by Landsat/ETM+, Terra/MODIS, ADEOS-II/GLI and 92 bands-CONTINUE sensors (Zhang *et al.*, 2003). The resulting pattern decomposition coefficients are independent of the sensor. That is, regardless of the sensor, the four coefficients are nearly the same for the same samples. The average estimation error of reduced χ^2 values for Landsat/TM (ETM+), Terra/MODIS, ADEOS-II/GLI and CONTINUE sensors is 0.025 (Zhang *et al.*, 2004).

Conventional PDM can be explained using both spectral mixing analysis and multi-dimensional analysis (Zhang *et al.*, 2004). In the UPDM, the non-negative constraint for the coefficient solution is removed. The UPDM is a multi-dimensional analysis wherein standard patterns are interpreted as an oblique coordinate system, and coefficients are the coordinates of a pixel’s reflectance. In the UPDM, therefore, each pixel in a multi-spectral image is an observation vector that can be projected to a subspace that consists of standard water, vegetation, and soil patterns. Supplemental patterns can be included when necessary (Zhang *et al.*, 2004). This approach includes an orthogonal independent space, as any data in the multi-dimensional space can be approximated as a vector in this three- (or four-) dimensional standard subspace.

The ultimate goal is to apply the UPDM to satellite data. UPDM analyses using satellite data are more intricate than those using ground-measured data because of the presence of the atmosphere. Previous UPDM studies used about 600 ground samples (Zhang *et al.*, 2004). However, even this number of samples cannot cover all ground objects. This study validated the sensor-independent characteristics of the UPDM using MODIS and ETM+ satellite data from over the Three Gorges region in China, and assessed the independence of a vegetation index based on the universal pattern decomposition method (VIUPD) (Zhang *et al.*, 2004) using MODIS and ETM+ data.

2. The universal pattern decomposition method

Previous studies have discussed PDM (Fujiwara *et al.*, 1996; Muramatsu *et al.*, 2000; Daigo *et al.*, 2004) and UPDM (Zhang *et al.*, 2003, 2004) algorithms. The UPDM decomposes reflectance values at each pixel into a linear sum of standard spectral patterns for water, vegetation, soil and any supplemental patterns using the following formula (Zhang *et al.*, 2004):

$$R_i \rightarrow C_w \cdot P_{iw} + C_v \cdot P_{iv} + C_s \cdot P_{is} \dotsc + C_4 \cdot P_{i4} \quad (1)$$

where R_i is the reflectance of band i measured on the ground (or by satellite sensor), C_w , C_v and C_s are the respective decomposition coefficients, and P_{iw} , P_{iv} , and P_{is} are the standard spectral patterns of water, vegetation and soil normalized with respect to the properties of each sensor. C_4 represents

supplemental coefficients. In this case, a yellow-leaf spectrum is used, but the supplemental pattern is not fixed. Rather, it depends on the study purpose. P_{i4} is the supplementary standard pattern for i bands and is an optional component that is also controlled by the purpose of the study.

Equation (1) can be expressed using matrix notation as follows:

$$\begin{pmatrix} R_1 \\ R_2 \\ \vdots \\ R_n \end{pmatrix} = \begin{pmatrix} P_{1w} & P_{1v} & P_{1s} & P_{14} \\ P_{2w} & P_{2v} & P_{2s} & P_{24} \\ \vdots & \vdots & \vdots & \vdots \\ P_{nw} & P_{nv} & P_{ns} & P_{n4} \end{pmatrix} \cdot \begin{pmatrix} C_w \\ C_v \\ C_s \\ C_4 \end{pmatrix} + \begin{pmatrix} r_1 \\ r_2 \\ \vdots \\ r_n \end{pmatrix} \quad (2)$$

or
$$\mathbf{R} = \mathbf{P}\mathbf{C} + \mathbf{r} \quad (3)$$

where $\mathbf{R} = [R_1, R_2, \dots, R_n]^T$ is the column vector of observations, n is the number of spectral bands; $\mathbf{P} = [\mathbf{P}_w, \mathbf{P}_v, \mathbf{P}_s, \mathbf{P}_4]$ is the $n \times 4$ matrix of which the row vector is the standard spectral pattern for band number n , $\mathbf{C} = [C_w, C_v, C_s, C_4]^T$ is the column vector of UPDM coefficients and \mathbf{r} is the residual column vector for band i . Inverting (3) and minimizing the sum-of-squared-error criterion function (Duda, *et al.*, 2001) yields

$$\mathbf{J}_s = \|\mathbf{R} - \mathbf{P}\mathbf{C}\|_2^2 \quad (4)$$

This function can be solved by a gradient search procedure, as below:

$$\nabla \mathbf{J}_s(\mathbf{C}) = \frac{\partial (\mathbf{R} - \mathbf{P}\mathbf{C})^T (\mathbf{R} - \mathbf{P}\mathbf{C})}{\partial \mathbf{C}} \quad (5)$$

and setting it equal to zero. The unique solution of \mathbf{C} is

$$\mathbf{C} = (\mathbf{P}^T \mathbf{P})^{-1} \mathbf{P}^T \mathbf{R} \quad (6)$$

where \mathbf{R} is a vector known from satellite data, and \mathbf{P} is a standard spectral pattern matrix as described above. The spectral pattern matrix is derived from normalized standard spectral patterns of water, vegetation, soil, and supplementary data, which in this case is yellow leaf (Zhang *et al.*, 2004).

Spectral reconstruction precision was evaluated using reduced Chi-square values that satisfied the expression

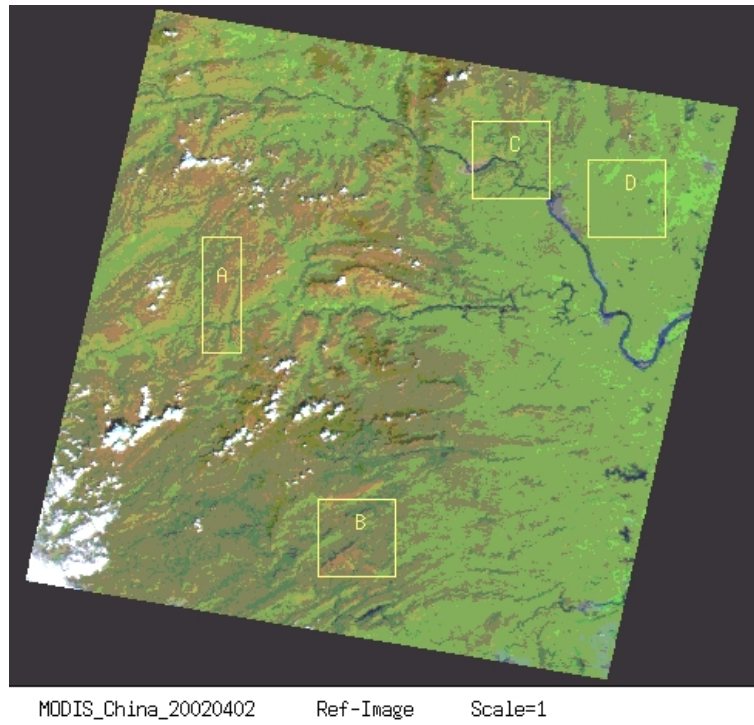
$$\chi^2 = \sum_{u=1}^n r(i)^2 / (n - 4) \quad (7)$$

Here, n is the number of bands, and r is the error of band i .

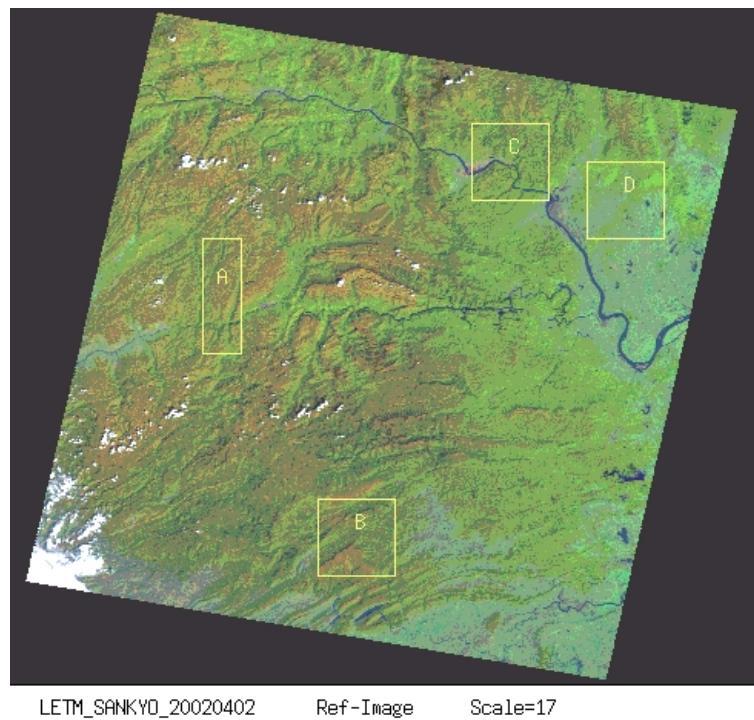
3. Data Processing

3.1 Data used in this analysis

Landsat /ETM+ standard product data (path 125/row 39) observed over the Three Gorges region of China on 2 April 2002 were acquired from the Beijing Remote Sensing Ground Station. Data are geo-referenced with a spatial resolution of 28.5 m. The solar zenith angle was 35.3° , and the observation time was 10:00 LT.



(a) MODIS image



(b) ETM+ image

Figure 1. MODIS and ETM+ reflectance image acquired over the Three Gorges region of China on 2 April 2002. Selected areas A, B, C, D refer to areas from alpine regions to hilly regions without cloud influences, (a) MODIS band 5, 4, 1 is displayed as red, green, blue, respectively, and (b) ETM+, band 6, 4, 1 is displayed as red, green, blue, respectively. The observed time of MODIS and ETM+ is 11:18 and 10:00, respectively.

Terra/MODIS data acquired over the same region on 2 April 2002 at 11:18 LT were provided by the MODIS Receiving Station at Wuhan University. MODIS bands 1 and 2 have horizontal resolutions of 250 m, and bands 3–7 have horizontal resolutions of 500 m; the average solar zenith angle is around 34.0°. MODIS L1B data contain geometric distortions that are reduced by geometric correction using the common nearest neighbor approach described in many studies. In this method, DN values are not changed, although a half-pixel shift in the output image space can occur (Lillesand, *et al.*, 2000). Each corrected pixel in the output image is geometrically similar to ETM+ data. This study used MODIS bands 1 to 7 re-sampled to a spatial resolution of 484.5 m, 17 times the resolution of ETM data (28.5 m). Figure 1 shows reflectance images for MODIS (a) and ETM+ (b) data for selected areas A, B, C and D, where terrain conditions vary by area.

ETM+ data are standard products that have better geo-referencing and geometric corrections. Thus, spatial re-sampling was applied to the data to match re-sampled MODIS data (at 484.5 m resolution).

The MODIS and ETM data covered the same region, between 29.35° and 31.28° N and 109.52° and 112.00° E, on the same observed date. Observation times differed by about an hour and the solar zenith angle was similar. Periodic noise from a mechanical sensor is present every 20 lines in MODIS band 5 (1230.0~1250.0 nm) but was ignored; this noise had little effect on the results of the analysis.

3.2 Radiometric correction and reflectance retrieval

Radiometric corrections to surface reflectance allow quantitative comparisons with spectral target signatures. Satellite sensors record total reflected energy and output the value as an electric signal that is called a DN value. The calibration task is to retrieve satellite radiances.

Radiance values for each ETM+ pixel in each band can be derived from the digital number (DN) according to (Joachim *et al.*, 1991)

$$L_{(ETM)} = a_{0(ETM)} + a_{1(ETM)} DN \quad (8)$$

MODIS radiances are (NASA, 2000)

$$L_{(MODIS)} = a_{1(MODIS)} (DN - a_{0(MODIS)}) \quad (9)$$

Here, L is the total radiance for the ETM+ and MODIS sensors at the satellite, in $mW \cdot cm^{-2} \cdot sr^{-1} \cdot \mu m^{-1}$; calibration constants a_0 and a_1 are offsets and gains for the ETM+ and MODIS sensors and are provided by data distribution agencies.

Radiation is scattered as it passes through and interacts with the atmosphere. Typically, total radiance is the sum of target-reflected radiance and Rayleigh scattering-caused path radiance (Muramatsu *et al.*, 2000). Radiometric correction in this case means removing the effects of Rayleigh scattering. Various atmospheric correction methods can be applied (Zhang *et al.*, 1998). More precise techniques use a statistical analysis of automatically masked invariant scene elements to derive a linear band-to-band transformation function (Schott *et al.*, 1986). However,

statistical methods give no quantitative measure of actual properties, so the present study uses a simplified Rayleigh scattering correction that ignores environmental scattering. Atmospheric Rayleigh scattering path radiance is approximated by

$$L_r = \frac{1}{4\pi} \cdot \frac{\mu_0}{\mu + \mu_0} \{1 - e^{-\tau_r \cdot (\frac{1}{\mu} + \frac{1}{\mu_0})}\} P_r(\varphi) \frac{E_0}{d^2} \quad (10)$$

where L_r is the Rayleigh scattering path radiance, in $\text{mW} \cdot \text{cm}^{-2} \cdot \text{sr}^{-1} \cdot \mu\text{m}^{-1}$, and μ_0 and μ represent the cosines of the sun zenith angle θ_0 and satellite zenith angle θ , respectively. E_0 is the solar irradiance at the top of the atmosphere, in $\text{mW} \cdot \text{cm}^{-2} \cdot \mu\text{m}^{-1}$, and d is the earth–sun distance in astronomical units. $P_r(\varphi)$ is the Rayleigh scattering phase function and can be written as

$$P_r(\varphi) = \frac{3}{4}(1 + \cos^2 \varphi) \quad (11)$$

with backscattering angle

$$\varphi = 180 - \theta_0 \quad (12)$$

τ_r is the molecular optical thickness for a standard Rayleigh atmosphere (Joachim *et al.*, 1991):

$$\tau_r = 0.00879\lambda^{-4.09} \quad (13)$$

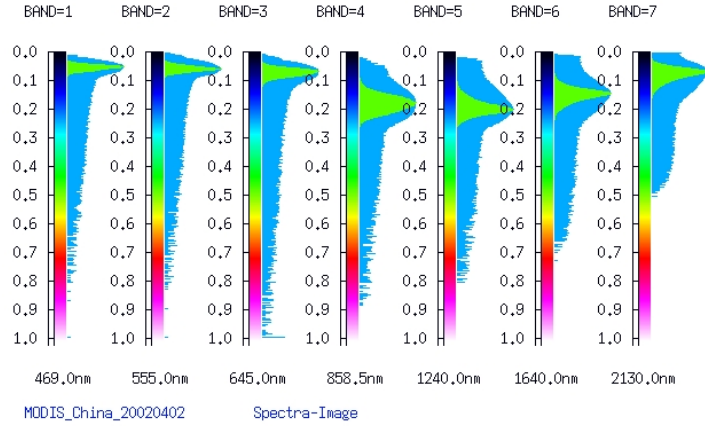
Solving for path radiance yields an equation for ground-target reflectance ρ_λ :

$$\rho_\lambda = \frac{\pi \cdot d^2 \cdot (L - L_r)}{E_{0\lambda} \cdot \cos \theta_0} \quad (14)$$

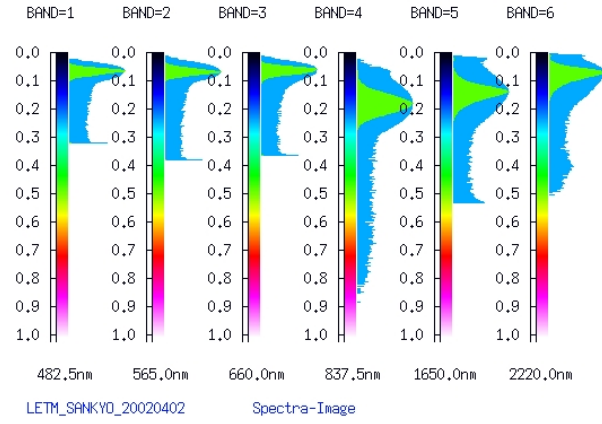
For MODIS reflectance at the top of the atmosphere, we can also compute ground-target reflectance using reflectance gain and offset in the MODIS L1B products (Zhang *et al.* 2005):

$$\rho_{\lambda(\text{MODIS})} = \frac{m_{R,\lambda}(DN_\lambda - b_{R,\lambda})}{\cos \theta_0} \quad (15)$$

Here, $m_{R,\lambda}$ and $b_{R,\lambda}$ are reflectance gain and offset. The path reflectance value computed by Rayleigh scattering path radiance is then removed. Table 1 shows Rayleigh scattering reflectance values for the MODIS and ETM+ sensors. Figure 2 shows spectra of MODIS and ETM+ data using values listed in Table 1 band by band. Blue represents the logarithmic value of reflectance for each pixel. Green represents the reflectance frequency.



(a) MODIS



(b) ETM+

Figure 2. MODIS and ETM+ ground-target reflectance histogram in respect to Figure 1. (a) MODIS (b) ETM+; blue represents the logarithmic value of reflectance for each pixel. Green represents the reflectance frequency.

Table 1 Rayleigh scattering correction values for MODIS and ETM+

Band	MODIS			ETM+		
	Wavelength nm	E_0 W/m ² /μm/sr	Rayleigh scattering	Wavelength nm	E_0 W/m ² /μm/sr	Rayleigh scattering
1*	459.0~479.0	2088.039	0.060	450.0~515.0	1969.0	0.055
2*	545.0~565.0	1865.903	0.033	525.0~605.0	1840.0	0.031
3	620.0~670.0	1607.099	0.019	630.0~690.0	1551.0	0.017
4	841.0~876.0	992.098	0.006	775.0~900.0	1044.0	0.007
5	1230.0~1250.0	474.399	0.001	1550.0~1750.0	225.7	0.000
6*	1628.0~1652.0	240.205	0.000	2090.0~2350.0	82.1	0.000
7	2105.0~2135.0	90.336	0.000			

*In this study, for convenience, we changed the MODIS band 1, 2 to band 3, 4 according to the wavelength value; for ETM+, we changed band 7 to band 6, respectively. The earth-sun distance on 2 April was 0.999910 (Zhang, *et al.* 2005) in astronomical units (149.6×10^6 km); the Rayleigh scattering value is expressed by the reflectance value.

3.3 UPDM subspace projection

Reflectance values for each pixel in multi-dimensional space were projected to four-dimensional UPDM space to transform the standard spectral pattern from the normalized standard spectral pattern at wavelengths between 350 nm and 2500 nm. For the MODIS sensor, the standard spectral vector is

$$\mathbf{P}_w = \begin{bmatrix} 3.336933 \\ 2.878424 \\ 1.542390 \\ 0.797594 \\ 0.230624 \\ 0.264724 \\ 0.114276 \end{bmatrix}, \mathbf{P}_v = \begin{bmatrix} 0.163671 \\ 0.465862 \\ 0.188812 \\ 2.327511 \\ 1.909090 \\ 1.035108 \\ 0.358373 \end{bmatrix}, \mathbf{P}_s = \begin{bmatrix} 0.517848 \\ 0.758124 \\ 0.918608 \\ 0.972886 \\ 1.080348 \\ 1.253452 \\ 1.255247 \end{bmatrix}, \mathbf{P}_4 = \begin{bmatrix} -1.771638 \\ 0.568648 \\ 2.501290 \\ 0.015900 \\ 0.208386 \\ -0.634276 \\ -1.124477 \end{bmatrix}$$

The vector for the ETM+ sensor is

$$\mathbf{P}_w = \begin{bmatrix} 3.277077 \\ 2.672011 \\ 1.449789 \\ 0.817368 \\ 0.219794 \\ 0.205009 \end{bmatrix}, \mathbf{P}_v = \begin{bmatrix} 0.175195 \\ 0.384025 \\ 0.171269 \\ 2.311455 \\ 0.961035 \\ 0.332513 \end{bmatrix}, \mathbf{P}_s = \begin{bmatrix} 0.545911 \\ 0.786754 \\ 0.925836 \\ 0.979686 \\ 1.251477 \\ 1.164075 \end{bmatrix}, \mathbf{P}_4 = \begin{bmatrix} -1.259582 \\ 0.957375 \\ 2.589210 \\ 0.023746 \\ -0.604368 \\ -1.392741 \end{bmatrix}$$

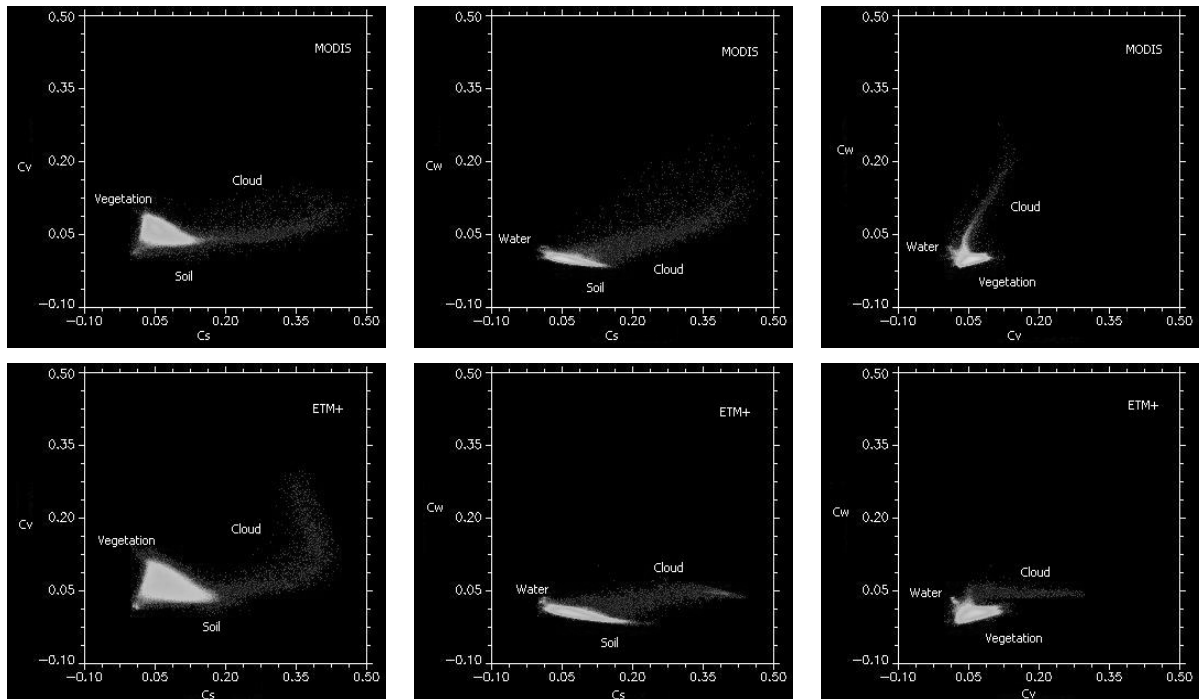


Figure 3. MODIS and ETM+ multispectral reflectance data expressed in the UPDM dimensional space. Upper rows from left to right are MODIS data expressed by Cs-Cv, Cs-Cw, Cv-Cw two dimensional spaces; lower rows are ETM+ data.

UPDM coefficient vectors were computed for each pixel using Equation (6). Multispectral data in multidimensional space were projected to four UPDM dimensional space. The UPDM vector in the new dimensional space has lower band-by-band correlation coefficients than the original dimensional space. Figure 3 shows MODIS and ETM+ data in UPDM space. For convenience, four-dimensional space is expressed via two-dimensional space of Cs, Cv and Cw, respectively, in Figure 3. The long tail represents clouds that differ between MODIS and ETM+ data owing to the one-hour difference in observation times. Figure 1 shows more cloud in the MODIS data than in the ETM+ data. Cloud-free regions are almost the same in the sensor-independent UPDM space.

4. Results and Discussion

4.1 Linear relationship of UPDM coefficients as a function of spatial resolution

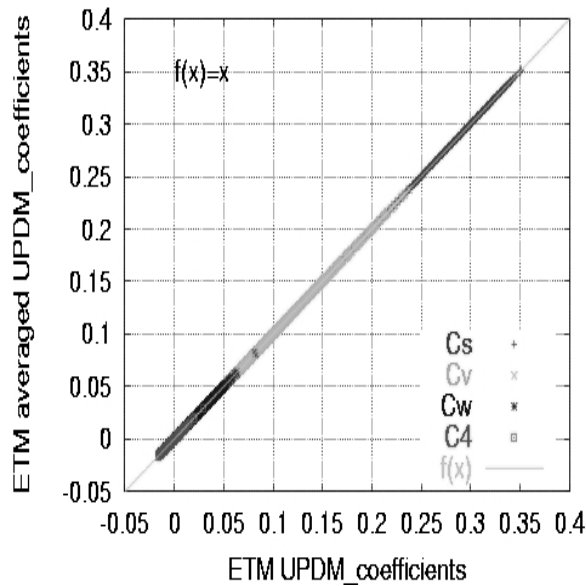


Figure 4. Relation between UPDM coefficients computed using ETM+ data with different spatial resolutions. The horizontal axis represents the UPDM coefficients computed from pixels with 484.5-m resolution, and the vertical axis represents the average values of UPDM coefficients using 17×17 pixels, which were computed from 28.5-m resolution ETM+ data.

UPDM coefficients show a linear relationship with data computed using different spatial resolutions. In this study, we computed UPDM coefficients using ETM+ data that were re-sampled to a horizontal resolution of 484.5 m. Of course, we could have used data with a horizontal resolution of 28.5 m and then computed the average value of the UPDM coefficients using 17×17 pixels ($28.5 \times 17 = 484.5$). Figure 4 shows the linear relationship between these two UPDM coefficients. The horizontal axis represents the UPDM coefficients computed from pixels with 484.5-m resolution, and the vertical axis represents the average values of UPDM coefficients using 17×17 pixels, which were computed from 28.5-m resolution ETM+ data.

4.2 Sensor independence of UPDM coefficients

Because UPDM is a sensor-independent method, UPDM coefficients derived from different sensors should have the same approximate values, at least theoretically. Previous studies using ground-measured data support this statement (Zhang *et al.*, 2004). UPDM coefficients computed in this paper use MODIS and ETM+ data acquired over the Three Gorges region on 2 April 2002. The relationship between coefficients was compared in four selected areas (A, B, C, and D) where topography varied from mountainous to hilly, as shown in Figure 1. Figure 5 shows the comparison. Linear regression equations are (a) $f(x) = 1.0103x$, (b) $f(x) = 0.9963x$, (c) $f(x) = 1.0057x$, and (d) $f(x) = 1.0077x$. Region D shows a linear relationship and the smallest root mean square (rms) value. Area D is the most sensor independent because it is the area in which terrain has the least influence.

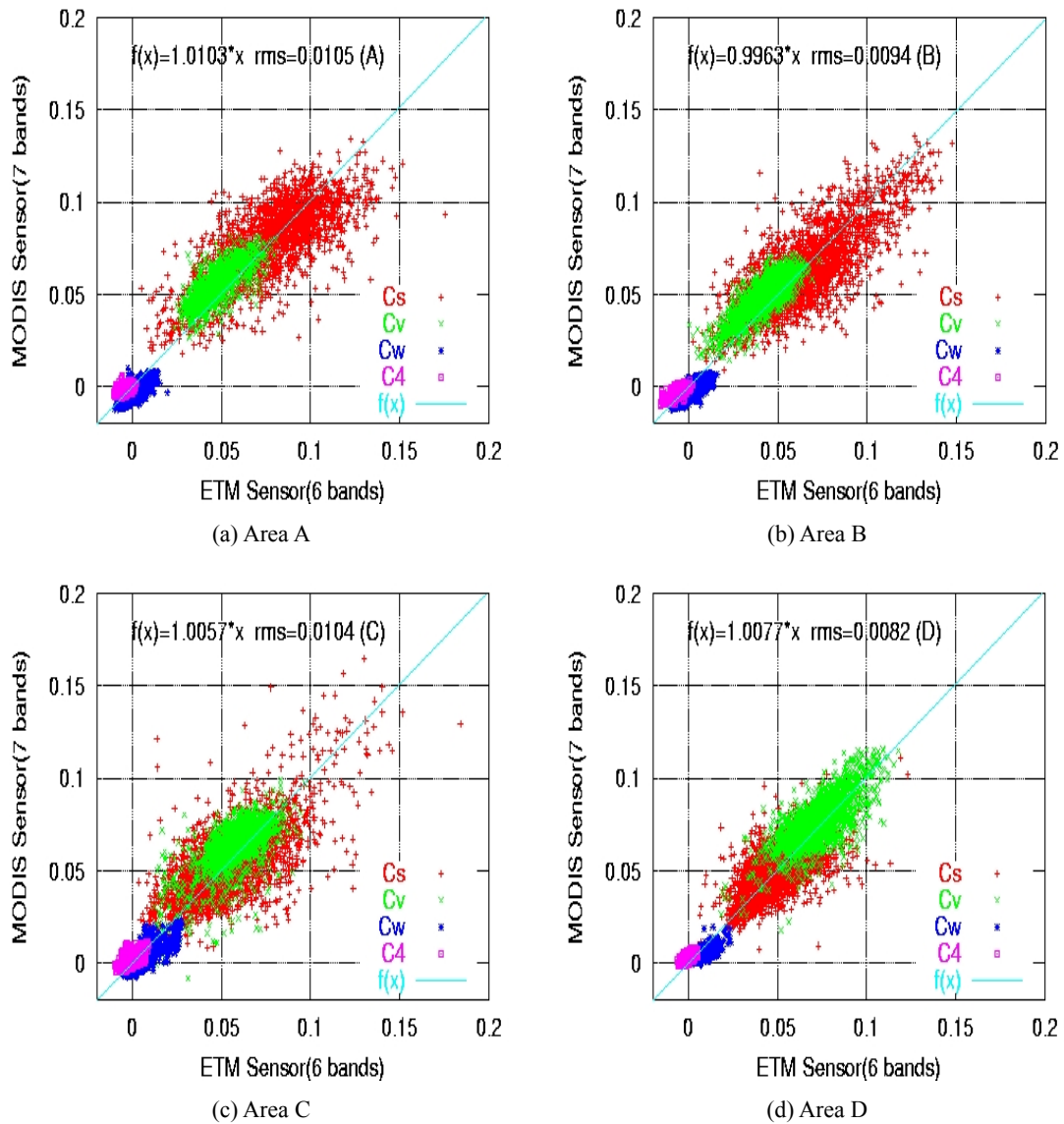


Figure 5. Correlation of the UPDM coefficients between MODIS and ETM+ sensor data. (a) area A with 1875 pixels, (b) area B with 2500 pixels, (c) area C with 2500 pixels, and (d) area D with 2500 pixels.

Table 2. (a) Linear regression parameter for area A using MODIS and ETM+ data

UPDM coefficients			Linear regression function	
coefficients	coefficient values	rms	vegetation function	rms
Cw	0.4808	0.0047	VIUPD: $f(x) = 1.0332x$ NDVI: $f(x) = 0.8860x$ EVI: $f(x) = 0.8031x$	0.0633
Cv	1.1496	0.0072		0.0392
Cs	0.9705	0.0170		0.0250
C4	0.3088	0.0012		
Σ	1.0103	Coefficients function: $f(x) = 1.0103 x$		0.0105

Table 2. (b) Linear regression parameter for area D using MODIS and ETM+ data

UPDM coefficients			Linear regression function	
coefficients	coefficient values	rms	vegetation function	rms
Cw	0.3247	0.0032	VIUPD: $f(x) = 1.0666x$ NDVI: $f(x) = 0.9243x$ EVI: $f(x) = 0.8261x$	0.0636
Cv	1.1432	0.0066		0.0369
Cs	0.9414	0.0146		0.0233
C4	0.3923	0.0013		
Σ	0.9963	Coefficients function: $f(x) = 0.9963 x$		0.0094

Table 2. (c) Linear regression parameter for area C using MODIS and ETM+ data

UPDM coefficients			Linear regression function	
coefficients	coefficient values	rms	vegetation function	rms
Cw	0.4320	0.0031	VIUPD: $f(x) = 1.0312x$ NDVI: $f(x) = 0.9204x$ EVI: $f(x) = 0.8262x$	0.0917
Cv	1.0870	0.0010		0.0689
Cs	0.9356	0.0161		0.0431
C4	0.2468	0.0018		
Σ	1.0057	Coefficients function: $f(x) = 1.0057 x$		0.0104

Table 2. (d) Linear regression parameter for area D using MODIS and ETM+ data

UPDM coefficients			Linear regression function	
coefficients	coefficient values	rms	vegetation function	rms
Cw	0.5696	0.0017	VIUPD: $f(x) = 1.0089x$ NDVI: $f(x) = 0.9137x$ EVI: $f(x) = 0.8130x$	0.0696
Cv	1.0427	0.0097		0.0409
Cs	0.9540	0.0114		0.0334
C4	-0.0693	0.0028		
Σ	1.0077	Coefficients function: $f(x) = 1.0077 x$		0.0082

Table 2 shows details of the UPDM coefficients for the two satellite sensors in each of the four areas. The table includes correlations, linear regression coefficients and vegetation index correlations. Of the four UPDM coefficients, Cv and Cs show linear behavior, whereas Cw and C4 do not, because Cw and C4 values are very small. A minor change caused by a pixel shift or topographic influence may

cause a relatively large shift in value. Figure 5 shows C_w and C_4 values clustered around zero; a small shift in values will move the linear regression coefficients away from the line $f(x) = x$. Figure 5 also shows somewhat larger rms values because of the re-sampling method for MODIS data. MODIS pixels may include a half-pixel shift, so pixels in MODIS and ETM+ data may not be identical. Such an effect is reduced by comparing 3×3 pixel averages of UPDM coefficients. Figure 6 shows the results of that comparison.

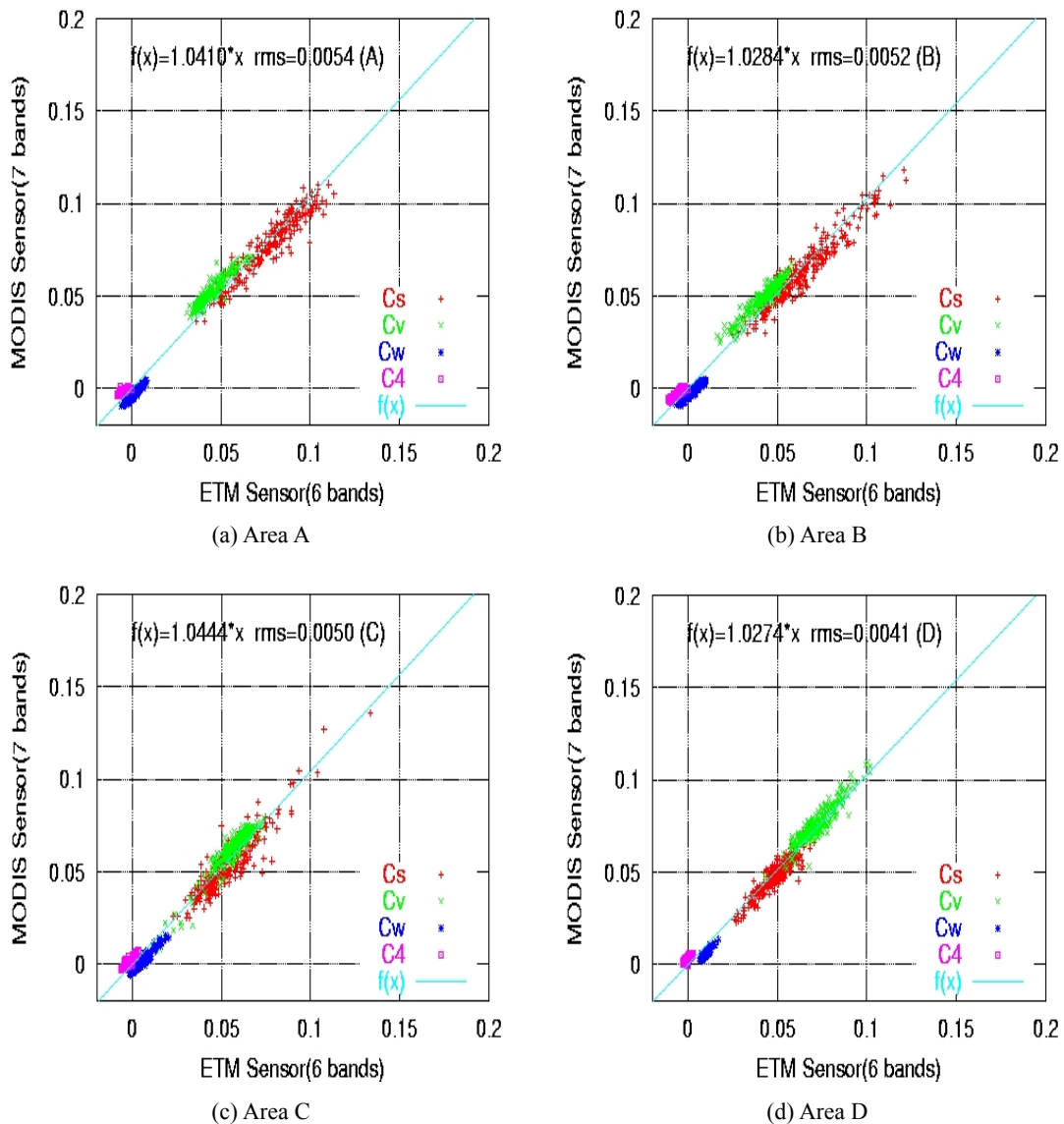


Figure 6. Correlation of the UPDM coefficients computed using average values of 3×3 pixels between MODIS and ETM+ sensor. (a) area A with 200 pixels, (b) area B with 256 pixels, (c) area C with 256 pixels, (d) area D with 256 pixels.

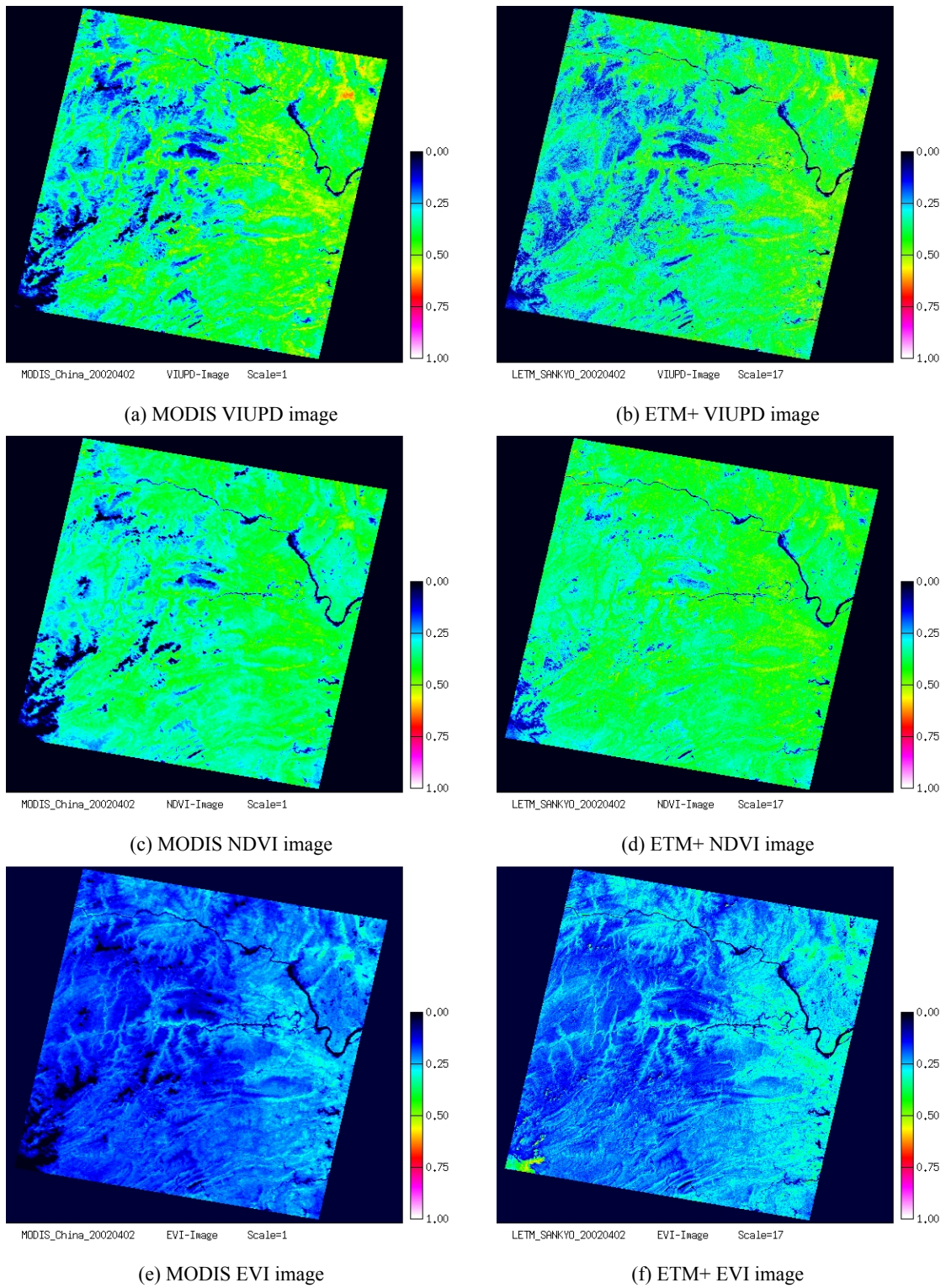


Figure 7 Vegetation index images computed from MODIS and ETM+ data. (a), (c) and (e) are the vegetation indices using VIUPD, NDVI, and EVI for the MODIS sensor, and (b), (d) and (f) are the vegetation indices using VIUPD, NDVI, and EVI for the ETM+ sensor.

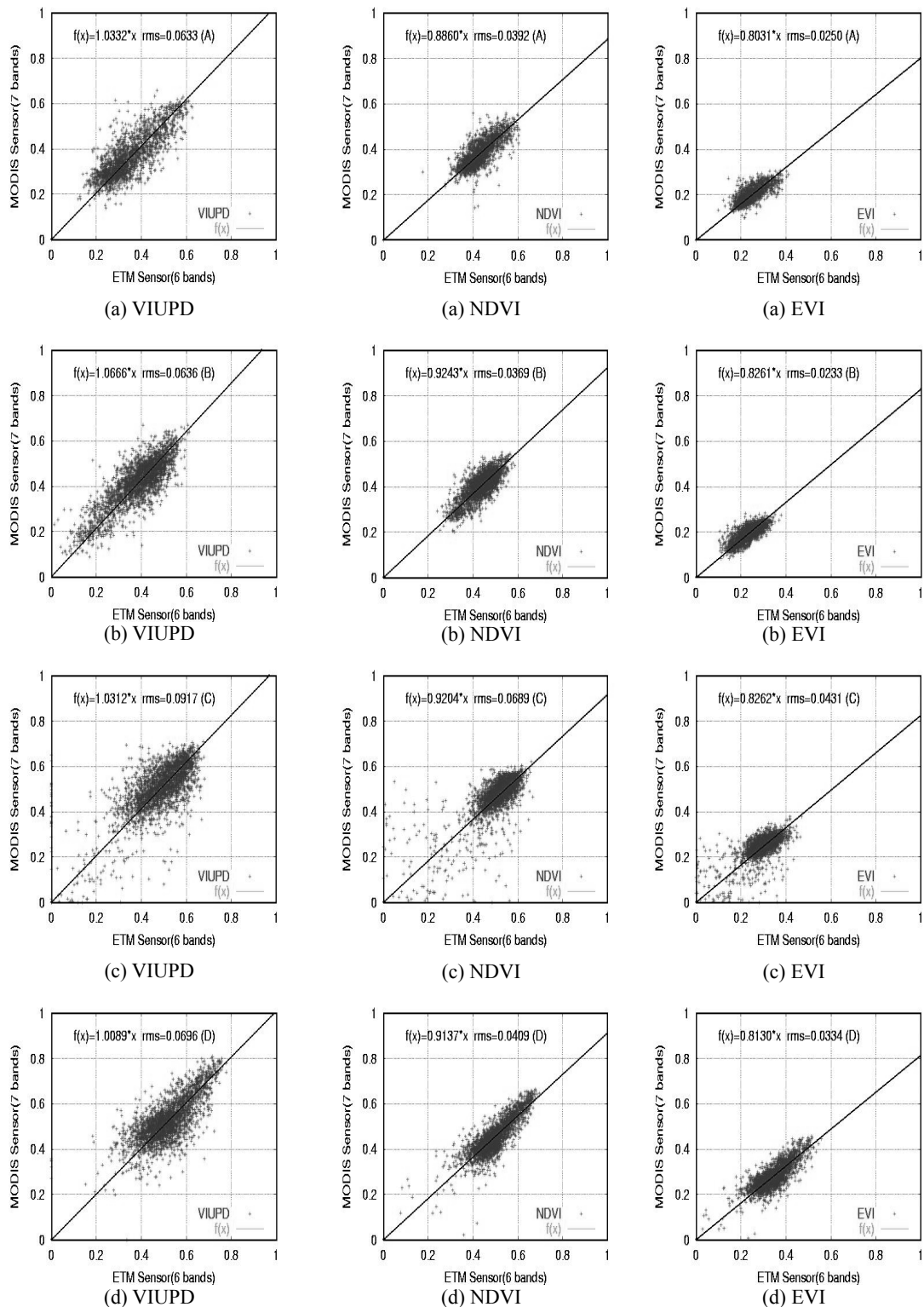


Figure 8 Correlations of MODIS and ETM+ vegetation indices. Columns denote values computed from selected areas (A, B, C and D) in Figure 1; rows refer to the vegetation index (VIUPD, NDVI, and EVI) obtained from data in the same areas.

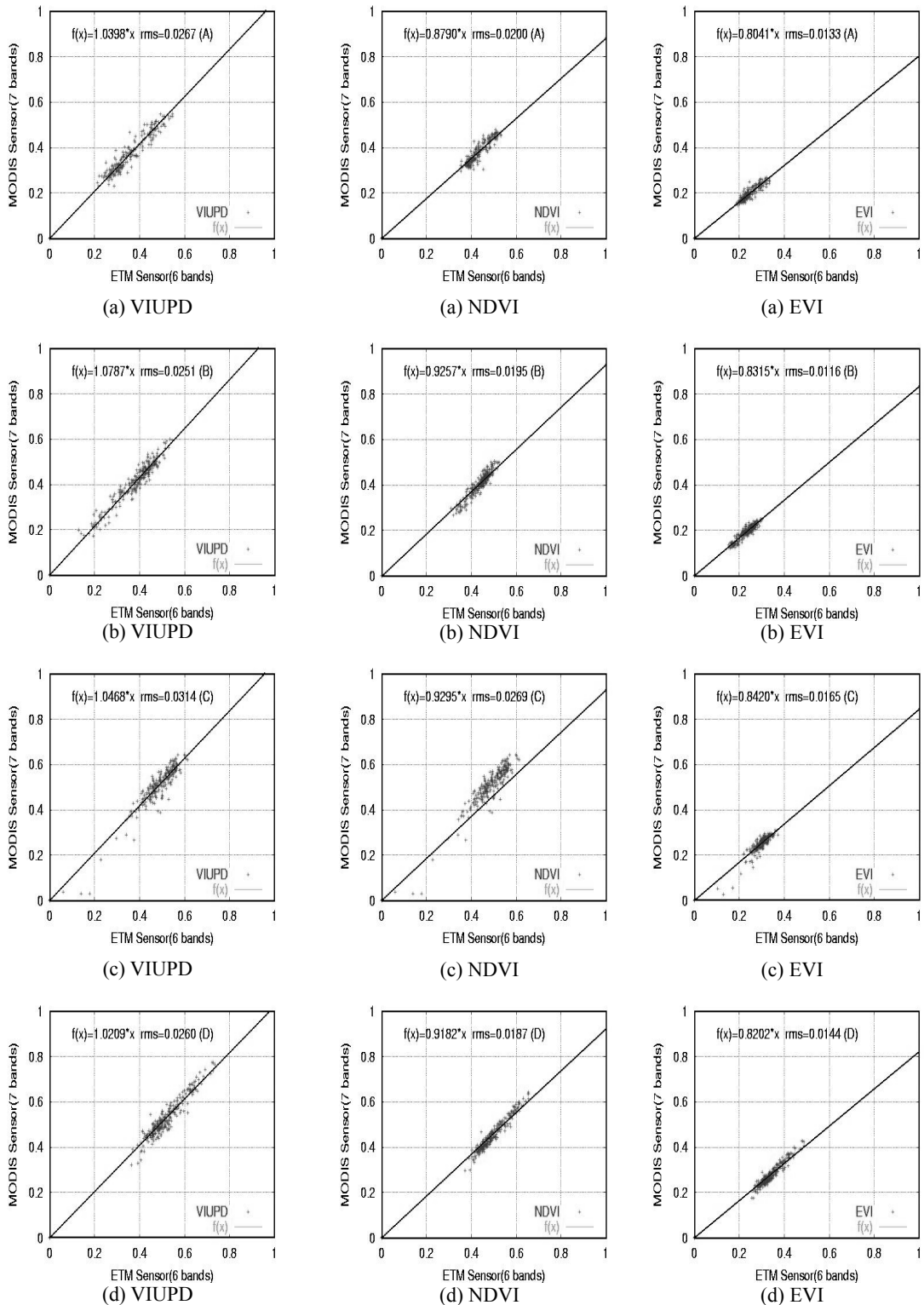


Figure 9 Correlations of MODIS and ETM+ 3×3 averaged vegetation indices. Columns denote values computed from selected areas (A, B, C, and D) in Figure 1; rows refer to the vegetation index (VIUPD, NDVI, and EVI) obtained from data in the same areas.

4.3 Sensor independence of vegetation index

A new vegetation index has been proposed based on the universal pattern decomposition method (VIUPD) (Zhang, *et al.*, 2004) and derived from sensor-independent UPDM coefficients. Previous studies have shown that the VIUPD is sensor independent. Table 2 compares the three vegetation indices. Figure 7 shows the three vegetation indices (VIUPD, NDVI, and EVI) computed from MODIS and ETM+ data. VIUPD images from MODIS and ETM+ show more detailed information than NDVI and EVI images, and the VIUPD images derived from MODIS and ETM+ data are similar. Figure 8 shows correlations between vegetation indices using data in the selected areas in Figure 1. Columns in the figure are for areas A, B, C and D as noted in Figure 1; rows denote the vegetation index: VIUPD, NDVI, and EVI. Two points stand out, namely the linear correlation and the smaller rms values. From area A to area D, VIUPD increases in independence: area D has a rms of 0.0696 and a regression function of $f(x) = 1.0089x$, a function which is the most linear relationship found in this study. Values with even smaller rms values are shown in Figure 9, which shows vegetation indices computed with 3×3 pixel averages.

5. Conclusion

Four UPDM coefficients were computed using Landsat /ETM+ and Terra/MODIS data observed over the Three Gorges region. Vegetation indices were computed in the same multi-dimensional space. UPDM coefficients computed with 6-band ETM+ data, with wavelengths between 350 and 2500 nm (the solar reflected wavelength region), were compared to coefficients computed with MODIS data in bands 1 to 7. Both datasets were re-sampled to a spatial resolution of 484.5 m. The DN value was converted to a reflectance value by considering radiometric calibration and atmospheric correction. Reflectance values are the input vector for calculating UPDM coefficients. Data processing precision depends on the algorithm selected. Because the aim of the present study was to assess the sensor independence of the UPDM, an easy and fast method was selected to preprocess the data. Such a preprocessing method may impact the representativeness of UPDM coefficients and derived vegetation indices.

The four UPDM coefficients are independent of the sensor. The independence of C_s and C_v is better than C_w and C_4 , because both C_w and C_4 have values near zero. Consequently, any small bias will move them far from a linear line. The fitted errors of reduced chi-square calculated from (7) for MODIS data are 0.000698, 0.000549, 0.000475, and 0.000409 for areas A through D, respectively. Similarly, fitted errors for ETM+ data are 0.000339, 0.000296, 0.000228, and 0.000181 for areas A through D, respectively. UPDM coefficients and vegetation indices (VIUPD, NDVI, and EVI) were computed using 3×3 pixel averages to evaluate the effect of pixel spatial location errors. Coefficients and vegetation indices computed this way both showed smaller rms

values. ETM+ gives smaller fit errors than MODIS, because ETM+ standard products have more precise geometry. Results also suggest that the VIUPD is sensor-independent, especially in areas with little topographic influence, such as areas C and D.

Hyper-multi dimensional spectral data observed by any sensor can be projected to the universal three- (or four-) dimensional UPDM space. UPDM techniques can reduce spectral features, decrease data amounts and allow sensor-independent operations including land cover classification and calculation of a sensor-independent vegetation index. Analytic studies based on UPDM space are possible. Radiometric and geometric errors in any satellite data used must be small.

Acknowledgments

This work was supported under the ADEOS-II/GLI Project of the Japan Aerospace Exploration Agency (JAXA), the Academic Frontier Promotion Project of the Ministry of Education, Science, Sports, and Culture of Japan, the 973 Project of the People's Republic of China (Project Number 2003CB415205), and the National Natural Science Foundation of China (Project Number 40471088).

References

- Daigo, M., Ono, A., Fujiwara, N., and Urabe, R. (2004). "Pattern decomposition method for hyper-multi-spectral data analysis," *International Journal of Remote Sensing*, 25(6): 1153-1166.
- Duda, R. O., Hart, P. E., Stork, D. G. (2001). *Pattern Classification*, 2nd edition, (New York: John Wiley & Sons Inc.).
- Duggin, M. J., Piwinski, D., Whitehead, V., and Ryland, G. (1982). Scan-angle dependence of radiance recorded by the NOAA-AVHRR. *Proceedings SPIE*, (363): 98–101.
- DeFries, R. S., and Townshend, J. R. G., (1994). NDVI-derived land cover classifications at a global scale. *International Journal of Remote Sensing*, (15): 3567–3586.
- Davis, J. C. (1986). *Statistics and Data Analysis in Geology*, 2nd edition. (New York: John Wiley & Sons Inc.).
- Fujiwara, N., Muramatsu, K., Awa, S., Hazumi, A. and Ochiai, F. (1996). "Pattern expansion method for satellite data analysis," (in Japanese). *Journal of Remote Sensing Society of Japan*, 17(3): 17-37.
- Hodges, J., Morrow N., and Strahler, A. (2000). "Application of the MODIS global supervised classification model to vegetation and land cover mapping of Central America,"

- International Journal of Remote Sensing*, 21(6,7): 1115-1138.
- Joachim H, Boris S. (1991). "Radiometric correction of multitemporal Thematic Mapper data for use in agricultural land-cover classification and vegetation monitoring," *International Journal of Remote Sensing*, (12)7: 1471-1491
- Kenea, N. H. (2001). "Influence of desert varnish on the reflectance of gossans in the context of Landsat TM data, southern Red Sea Hills, Sudan," *International Journal of Remote Sensing*, 22(10): 1879-1894.
- Lillesand, T. M., Kiefer, R. W. (2000). *Remote Sensing and Image Interpretation*, 4nd edition, (New York: John Wiley & Sons Inc.).
- Muramatsu, K., Furumi, S., Fujiwara, N., Hayashi, A., Daigo, M., and Ochiai, F. (2000). "Pattern decomposition method in the albedo space for Landsat TM and MSS data analysis," *International Journal of Remote Sensing*, 21(1): 99-119.
- NASA, 2000. Members of the MODIS Characterization Support Team for NASA/Goddard Space Flight Center. MODIS Level 1B product Users Guide.
- Schott, J. R., Salvaggio, C., and Volchok, W. J. (1998). "Radiometric scene normalization using pseudoinvariant features," *Remote Sensing of Environment*, 26: 1-16.
- Teillet, P. M., Staenz, K., and Williams, D. J. (1997). "Effects of Spectral, Spatial, and Radiometric Characteristics on Remote Sensing Vegetation Indices of Forested Regions," *Remote Sensing of Environment*, 61: 139-149.
- Zhang, L., Mitsushita, Y., Furumi, S., Muramatsu, K., Fujiwara, N., Daigo, M., and Zhang, L. (2003). "Universality of modified Pattern Decomposition Method for satellite sensors," *Asia GIS Conference Publications*.
- Zhang, L., Furumi, S., Murumatsu, K., Fujiwara, N., Daigo, M., and Zhang, L. (2004). "Sensor-independent analysis method for hyper-multi spectra based on the pattern decomposition method," *International Journal of Remote Sensing*, (in review).
- Zhang, L., Furumi, S., Murumatsu, K., Fujiwara, N., Daigo, M., and Zhang, L. (2004). "A new vegetation index based on the Universal Pattern Decomposition Method," *International Journal of Remote Sensing*, (in review).
- Zhang, L., Li, D., Tong, Q., Zheng, L. (1998). "Calibration of airborne imaging spectrometer data acquired from Poyang Lake area, China," *Proceedings of SPIE*, (3502):57-64.
- Zhang, L., Zhang, L., Fujiwara, N., and Murumatsu, K. (2005). "Calculation of the terrestrial vegetation index VIUPD using MODIS data,"(in Chinese) *Journal of Geomatics and information science of Wuhan University, China*, (30)5:468-471.
- Zhang, L., Zhang, L., Fujiwara, N., and Murumatsu, K. (2005). "The universal pattern decomposition method based on the hyper spectral satellite remotely sensed data," (in

Chinese) *Journal of Geomatics and information science of Wuhan University, China*,
(30)3:264-268.

**The English in this document has been checked by at least two professional editors,
both native speakers of English. For a certificate, see:
<http://www.textcheck.com/cgi-bin/certificate.cgi?id=2ZaY26>**